Pergamon

PII: S0020-7225(96)00081-X

Int. J. Engng Sci. Vol. 35, No. 4, pp. 409–422, 1997

0020-7225/97 $17.00 + 0.00

AN ANALYSIS OF PULSATILE FLOW IN A MODEL AORTIC BIFURCATION

S. CHAKRAVARTY and P. K. MANDAL

Department of Mathematics, Visva-Bharati University, Santiniketan-731 235, India

Abstract—An appropriate geometry of the model aortic bifurcation in the presence of stenosis is developed in order to analyse the flow phenomenon in the bifurcated aorta owing to a pulsatile pressure gradient. The flow in this geometry is determined by the branching of the aorta and the existence of a reverse flow area in the daughter artery. The present analysis incorporates the arterial wall motion and its effect on local fluid mechanics. From the computational results one may disclose that the non-Newtonian rheology of blood does not change the flow patterns in the parent aorta, but their is a drastic change in their daughter artery, which in turn causes an appreciable increase in the shear stress on both the parent and its daughter arteries. The present geometry bears the potential for a better understanding of the flow characteristics in daughter arteries where a stationary zone is located near the outer wall and a flow separation in the inner wall vicinity. The agreement between the present results and the existing ones is found to be quite satisfactory. © 1997 Elsevier Science Ltd. All rights reserved.

1. INTRODUCTION

It is a well established fact that the study of blood flow in the aortic bifurcation is of great clinical interest both with respect to genesis and the diagnostics of atherosclerosis—an arterial disease leading to the malfunction of the cardiovascular system. Such arterial disease usually appears around curvatures, junctions and bifurcations of large and medium arteries, where the flow patterns are generally complicated. As a result of the complicated flow phenomenon, it is often difficult to distinguish these disturbances from flow characteristics occurring normally in these regions. It is believed that the arterial walls in these regions are exposed to both high and low shear stresses which are responsible for the adhesion and deposition of blood platelets and lipids. Liepsch and Moravec [1] and Liepsch [2] have pointed out from their experimental investigations that in regions with high shear stresses, the blood cells are damaged or their surface is changed and then the particles stick to the wall followed by a deposition in regions with low shear stresses.

Quite a good number of theoretical and experimental studies have been carried out to investigate the significant role of hemodynamics in atherogenesis. A comprehensive review relevant to the subject under study has been conducted appreciably by Lou and Yang [3]. However, there have been only a few experimenal investigations, to the authors' knowledge, performed to determine the effect of wall deformability on the wall shear stress and other local flow conditions in aortic bifurcations. Lou and Yang [4] have investigated the effect of vessel wall flexibility on the flow field at the aortic bifurcation numerically, from a computer simulation. A theoretical model minimizing pulse wave reflection by matching impedance through bifurcation has been developed by Brown [5]. The possibility of a continuous change in area from parent artery to the apex of bifurcations and into the branches has been incorporated in his model in order to evaluate the effect of branch angle on the mechanical properties of daughter vessels.

An attempt is made in the present theoretical investigation to evaluate some of the important characteristics of pulsatile blood flow in aortic bifurcation using an appropriate mathematical model. It is commonly believed that the effect of non-Newtonian property of the fluid representing blood is small in larger arteries, where the shear rate is high. However, low shear spots also exist near bends and bifurcations of the vessel. It has been suggested from experimental findings (cf. Lessner *et al.* [6], Thurston [7]) that human blood possesses significant viscoelastic properties in the frequency range of physiological importance which may be attributed to several factors. The dominant factors are the viscoelastic properties of

individual red cells and the internal structures by cellular interactions. The present study includes both the properties of Newtonian and non-Newtonian fluid in order to examine their effects on the flow mechanism in the arterial bifurcation. Special emphasis is put on the effect of wall motion on local fluid mechanics but not on the stresses and strains in the vessel wall. A suitable time-dependent geometry of the bifurcated vessel has been constructed and duly accounted for. The parent aorta is assumed to have a mild stenosis in its lumen while the daughter ones are free from any constriction. The bifurcation is considered to be symmetrical and the appropriate curvatures at the lateral junctions and the flow divider are introduced so as to make the geometrical shape realistic in a sense that when a vessel bifurcates, it does it gradually. Most of the existing numerical models (cf. Patil and Subbaraj [8], Nazemi *et al.* [9]) have sharp corners which can cause discontinuity and abnormal values in shear rates and can also induce large flow separation zones or produce otherwise non-existent flow separation zones. The governing equations of motion of the system are sought first in the Laplace transform space and their solutions are obtained subject to the appropriate boundary conditions by using a finite difference scheme. The use of the central difference formula and the Thomas algorithm help to determine the flow velocity, the flow rate and the wall shear stresses in both the parent and the daughter arteries in the transformed domain. Laplace inversion is carried out finally by Gauss quadrature formulae. A quantitative analysis for the important quantities is performed at the end of the paper through graphical display of the results and their discussion illustrates the applicability of the present model.

2. FORMULATION OF THE PROBLEM

For the mathematical analysis of the problem under consideration, the following assumptions are taken into account:

- The arteries forming bifurcations are symmetrical and straight circular cylinders of finite length.
- The parent aorta possesses a single mild stenosis in its lumen (cf. Clark *et al.* [10]).
- The arterial wall motion is introduced into the local fluid mechanics governing blood flow.
- Blood is a homogeneous Newtonian fluid of constant density.
- Curvatures are introduced at the lateral junctions and the flow divider so that one can rule out the possibility of the presence of any discontinuity causing non-existent flow separation zones.

Let (r, θ, z) be the coordinates of a material point in the cylindrical polar coordinate system where the z-axis is taken along the axis of the artery while r, θ are taken along the radial and the circumferential directions respectively. The geometry of the bifurcated artery (cf. Fig. 1) in

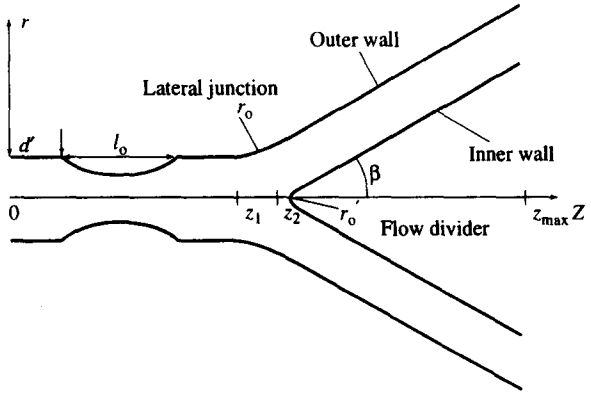

Fig. 1. Schematic diagram of the stenosed bifurcated artery.

the presence of stenosis is constructed mathematically of which the outer wall geometry is described by

$$R_1(z,t)=\begin{cases} a_1(t), & 0\le z\le d' \quad \text{and} \quad d'+l_0\le z\le z_1 \\ \left[a-\dfrac{4\tau_m}{l_0^2}(l_0(z-d')-(z-d')^2)\right]a_1(t), & d'\le z\le d'+l_0 \\ [a+r_0-\sqrt{r_0^2-(z-z_1)^2}]a_1(t), & z_1\le z\le z_2 \\ [2r_1\sec\beta+(z-z_2)\tan\beta]a_1(t), & z_2\le z\le z_{\max} \end{cases} \tag{1}$$

while that for the inner half is given by

$$R_2(z,t)=\begin{cases} 0, & 0\le z\le z_3 \\ \sqrt{r_0'^2-(z-z_3-r_0')^2}b_1(t), & z_3\le z\le z_3+r_0'(1-\sin\beta) \\ [r_0'\cos\beta+z_4]b_1(t), & z_3+r_0'(1-\sin\beta)\le z\le z_{\max} \end{cases} \tag{2}$$

where $R_1(z,t)$ and $R_2(z,t)$ are the respective radii of the outer and the inner wall, a the radius of the parent artery, r_1 the radius of the daughter artery, (r_0, r_0') the radii of curvatures for the lateral junction and the flow divider respectively, l_0 the length of the stenosis at a distance d' from the origin, z_1 the location of the onset of the lateral junction, z_2 the offset of the lateral junction, z_3 the apex, β, half the bifurcation angle and τ_m represents the maximum height of the stenosis at $z=d'+l_0/2$. Here, $z_{\max}$ designates the finite length of the bifurcated artery under consideration.

Moreover, the parameters involved in the above expressions (1) and (2) may be defined as

$$\left.\begin{aligned} a_1(t)&=1-(\cos\omega t-1)k\exp(-k\omega t), \\ b_1(t)&=\frac{1}{a_1(t)}, \\ z_2&=z_1+(a-2r_1\sec\beta)\frac{\sin\beta}{\cos\beta-1}, \\ z_4&=\{z-z_3-r_0'(1-\sin\beta)\}\tan\beta, \\ r_0&=\frac{(a-2r_1\sec\beta)}{\cos\beta-1}, \\ r_0'&=\frac{(z_3-z_2)\sin\beta}{1-\sin\beta} \end{aligned}\right\} \tag{3}$$

and $z_3=z_2+q$, where q is chosen to be a small number lying in the range $0.1\le q\le 0.5$ for compatibility of the geometry and k is a constant.

Let us consider the flow to be unsteady, axisymmetric, laminar, one dimensional and fully developed, the basic equation of motion governing such flow in the absence of any radial/rotational flow may be written as

$$\rho\frac{\partial w}{\partial t}=\mu\left(\frac{\partial^2 w}{\partial r^2}+\frac{1}{r}\frac{\partial w}{\partial r}\right)-\frac{\partial p}{\partial z}, \tag{4}$$

where $w=w(r,z,t)$ is the axial velocity of the flowing blood, p the pressure, ρ the density and μ the viscosity of blood.

Since we focus our attention on the axial flow behaviour of blood, we have further

$$\frac{\partial p}{\partial r}=0=\frac{\partial p}{\partial \theta}. \tag{5}$$

These relations yield $p = p(z, t)$. The form of the pressure gradient present in (4) appearing due to pumping action of the heart, has been taken from Burton [11] as

$$-\frac{\partial p}{\partial z} = A_0 + A_1 \cos(\omega t), \tag{6}$$

where A_0 is the constant amplitude of the presure gradient, A_1 is the amplitude of the pulsatile component giving rise to systolic and diastolic pressure; $\omega = 2\pi f_p$, f_p is the pulse frequency.

2.1 Boundary conditions

The velocity gradient of the streaming blood along the axis of the bifurcated artery till its apex may be assumed to be equal to zero, that is, there is no shear rate of the fluid along the axis, which may be written as

$$\frac{\partial w}{\partial r} = 0 \quad \text{on} \quad r = 0, \qquad 0 \leqslant z \leqslant z_3. \tag{7}$$

The velocity boundary condition on the outer wall is the usual no slip condition, given by

$$w(r, z, t) = 0 \quad \text{on} \quad r = R_1(z, t), \tag{8}$$

while that on the inner half (daughter) is also taken to be zero, that is,

$$w(r, z, t) = 0 \quad \text{on} \quad r = R_2(z, t), \qquad z_3 \leqslant z \leqslant z_{\max}. \tag{9}$$

Also, it is assumed that there is a non-zero velocity of the flowing blood when the system is at rest. That means

$$w(r, z, t) = w_0 \quad \text{at} \quad t = 0. \tag{10}$$

3. METHOD OF SOLUTION

Generally in a problem dealing with the coupling of the fluid mechanics with the vessel wall mechanics, $R_1(z, t)$ and $R_2(z, t)$ would not be given, but instead, could be computed as a part of the solution of the coupled problem. Here both $R_1(z, t)$ and $R_2(z, t)$ are prescribed and hence our attention is focused on the hemodynamic factors.

Introduce a radial coordinate transformation as an initial step, given by

$$\xi = \frac{r - R_2}{R_1 - R_2} = \frac{r - R_2}{R}, \tag{11}$$

which has the effect of immobilizing the bifurcated arterial wall in the transformed coordinate ξ. Here, $R(z, t) = R_1(z, t) - R_2(z, t)$.

Using this transformation, the equation (4) takes the following form:

$$\rho \frac{\partial w}{\partial t} = \mu \left[\frac{1}{R^2} \frac{\partial^2 w}{\partial \xi^2} + \frac{1}{R(\xi R + R_2)} \frac{\partial w}{\partial \xi} \right] - \frac{\partial p}{\partial z} + \frac{\rho}{R} \left(\xi \frac{\partial R}{\partial t} + \frac{\partial R_2}{\partial t} \right) \frac{\partial w}{\partial \xi}, \tag{12}$$

where $w = w(\xi, z, t)$.

The boundary conditions (7)–(10) are also transformed in concert with (11) to

$$\frac{\partial w}{\partial \xi} = 0 \quad \text{on} \quad \xi = 0 \quad \text{for} \quad z < z_3 \tag{13}$$

$$w(\xi, z, t) = 0 \quad \text{on} \quad \xi = 1 \tag{14}$$

$$w(\xi, z, t) = 0 \quad \text{on} \quad \xi = 0 \quad \text{for} \quad z \geqslant z_3 \tag{15}$$

$$w(\xi, z, 0) = w_0. \tag{16}$$

The last term appearing in the right hand side of (12) is associated with the wall motion of

the bifurcated artery. In order to solve (12) subject to the boundary conditions (13)–(16), these are all sought in the Laplace transform (L.T.) space of which (12) should be read as

$$\mu\left[\frac{1}{\bar{R}^2}\frac{\partial^2\bar{w}}{\partial\bar{\xi}^2}+\frac{1}{\bar{R}(\bar{\xi}\bar{R}+\bar{R}_2)}\frac{\partial\bar{w}}{\partial\bar{\xi}}\right]+\frac{\rho}{\bar{R}}[s(\bar{\xi}\bar{R}+\bar{R}_2)-\{\bar{\xi}R(z,0)+R_2(z,0)\}]\frac{\partial\bar{w}}{\partial\bar{\xi}}-\rho s\bar{w}$$
$$=\frac{\mathrm{d}\bar{p}}{\mathrm{d}z}-\rho w(\bar{\xi},z,0), \quad (17)$$

accompanied by the transform boundary conditions in the L.T. space. The quantities designated by a bar represent their Laplace transforms and s, the transformation variable.

4. FINITE DIFFERENCE APPROXIMATION

The finite difference scheme for solving (17) is based on the central difference formula to transform all the spatial derivatives in the L.T. space in the following manner:

$$\frac{\partial\bar{w}}{\partial\bar{\xi}}=\frac{\bar{w}_{i+1,j}-\bar{w}_{i-1,j}}{2\Delta\xi} \quad \text{and} \quad \frac{\partial^2\bar{w}}{\partial\bar{\xi}^2}=\frac{\bar{w}_{i+1,j}-2\bar{w}_{i,j}+\bar{w}_{i-1,j}}{(\Delta\xi)^2}.$$

Introducing these finite difference approximations of the spatial derivatives involved in (17) one can transform it to the following difference equation:

$$\left[\mu\left\{\frac{1}{\bar{R}_i^2(\Delta\xi)^2}+\frac{1}{\bar{R}_i(\bar{\xi}_j\bar{R}_i+\bar{R}_{2i})2\Delta\xi}\right\}+\frac{\rho}{\bar{R}_i}\{-R_{20i}+s\bar{R}_{2i}+\bar{\xi}_j(-R_{0i}+s\bar{R}_i)\}\frac{1}{2\Delta\xi}\right]\bar{w}_{i,j+1}$$
$$+\left[-\frac{2\mu}{\bar{R}_i^2(\Delta\xi)^2}-\rho s\right]\bar{w}_{i,j}+\left[\mu\left\{\frac{1}{\bar{R}_i^2(\Delta\xi)^2}-\frac{1}{\bar{R}_i(\bar{\xi}_j\bar{R}_i+\bar{R}_{2i})2\Delta\xi}\right\}\right.$$
$$\left.-\frac{\rho}{\bar{R}_i}\{-R_{20i}+s\bar{R}_{2i}+\bar{\xi}_j(-R_{0i}+s\bar{R}_i)\}\frac{1}{2\Delta\xi}\right]\bar{w}_{i,j-1}=\frac{\mathrm{d}\bar{p}}{\mathrm{d}z}-\rho w_0. \quad (18)$$

The above equation can be rewritten in a more compact form as

$$a_{i,j}\bar{w}_{i,j-1}+b_{i,j}\bar{w}_{i,j}+c_{i,j}\bar{w}_{i,j+1}=d_{i,j}, \quad (19)$$

where the respective expressions for $a_{i,j}$, $b_{i,j}$ and $c_{i,j}$ are included in the square brackets while that for $d_{i,j}$ is given on the right hand side of (18).

Equation (19) is of tridiagonal type and this can be solved by the Thomas algorithm where one defines $\bar{\xi}_j=(j-1)\Delta\xi$, $j=1(1)N+1$ and $z_i=(i-1)\Delta z$, $i=1(1)M+1$ for the entire bifurcated artery under consideration in which $\Delta\xi$ and Δz are the increments in the radial and the axial directions respectively. Also the boundary conditions (13)–(15) have their finite difference representations in the L.T. space, given by

$$\bar{w}_{i,1}=\bar{w}_{i,2} \quad \text{for} \quad z<z_3, \quad (20)$$

$$\bar{w}_{i,N+1}=0 \quad \forall i, \quad (21)$$

$$\bar{w}_{i,1}=0 \quad \text{for} \quad z\geqslant z_3. \quad (22)$$

After having obtained the axial velocity $\bar{w}_{i,j}$ in the transformed space, the volumetric flow rate $(\bar{Q}_\mathrm{p}, \bar{Q}_\mathrm{d})$ for both the parent $(z<z_3)$ aorta and the daughter $(z\geqslant z_3)$ arteries can be determined respectively in the L.T. space as

$$\bar{Q}_\mathrm{p}=2\pi\bar{R}_i\left[\bar{R}_i\int_0^1\bar{\xi}_j\bar{w}_{i,j}\,\mathrm{d}\bar{\xi}_j+\bar{R}_{2i}\int_0^1\bar{w}_{i,j}\,\mathrm{d}\bar{\xi}_j\right], \quad (23)$$

$$\bar{Q}_\mathrm{d}=\pi\bar{R}_i\left[\bar{R}_i\int_0^1\bar{\xi}_j\bar{w}_{i,j}\,\mathrm{d}\bar{\xi}_j+\bar{R}_{2i}\int_0^1\bar{w}_{i,j}\,\mathrm{d}\bar{\xi}_j\right]. \quad (24)$$

The resistance to flow $[(\bar{\lambda}_p)_i, (\bar{\lambda}_d)_i]$ both for the parent aorta and the daughter arteries in the transformed domain may be obtained as

$$(\bar{\lambda}_p)_i = \frac{\left| z_3 \frac{d\bar{p}}{dz} \right|}{\bar{Q}_p} \qquad (z < z_3), \tag{25}$$

$$(\bar{\lambda}_d)_i = \frac{\left| (z_{max} - z_3) \frac{d\bar{p}}{dz} \right|}{\bar{Q}_d} \qquad (z \geqslant z_3). \tag{26}$$

Finally, the wall shear stress $[(\bar{\tau}_p)_i, (\bar{\tau}_{od})_i]$ on the parent and the daughter external wall can be derived and computed right from equation (4) whose expressions are not shown here for the sake of brevity, while that on the inner wall of the daughter vessel may be obtained in the transformed space as

$$(\bar{\tau}_{id})_i = -\mu \frac{\bar{w}_{i,2}}{\bar{R}_i \Delta\xi} \quad \text{for} \quad z \geqslant z_3. \tag{27}$$

Here the suffixes "od" and "id" indicate the outer daughter and the inner daughter respectively.

Knowing all the solutions in the L.T. domain, the inversion is carried out numerically by means of Gaussian quadrature formulae in order to have their measure quantitatively in the physical domain and hence to perform a proper discussion of the results obtained in the following section.

5. NUMERICAL RESULTS AND DISCUSSION

In order to illustrate the applicability of the present mathematical model, the existing experimental data for the various physical parameters involved in this analysis have been employed. The numerical computations have been performed with the objectives to estimate the flow velocity, the flow rates and the wall shear stresses for both the parent aorta and its daughter arteries quantitatively. The effects of wall motion and blood rheology on those physical quantities in such a bifurcated flow phenomenon are estimated quantitatively. For this purpose, the followng data have been taken (Milnor [12]; Lou and Yang [3]): $a = 7.5$ mm, $l_0 = 15$ mm; $\dot{d}' = 5$ mm, $z_{max} = 60$ mm, $\tau_m = 0.4a$, $f_p = 1.2$ Hz, $\rho = 1.05 \times 10^3$ kgm^{-3}, $\mu = 0.035$ P, $\beta = 30°$, $z_4 = 25$ mm, $r_1 = 0.51a$, $A_0 = 100$ kg m^{-2} s^{-2}, $A_1 = 0.2\ A_0$, $k = 0.1$.

The finite difference scheme has been found to converge with the spacings $\Delta z = 0.01$ and $\Delta\xi = 0.005$. Numerical results are obtained for the flow velocity by solving the difference equation (19) subject to the conditions (20)–(22) where various grid sizes are chosen in order to achieve the convergence. It may be mentioned that the necessary convergence has been achieved with the desired degree of accuracy for a grid size of 600×200. The results thus obtained are finally shown through Figs 2–13 which help validate the applicability of the current mathematical model.

The results of the Fig. 2 illustrate the nature of the velocity profile of the streaming blood in the parent aorta at a specific locaiton of $z = 12.5$ mm corresponding to the maximum narrowing for different time periods. The present figure also includes the corresponding results—one by disregarding the wall motion and the other by incorporating non-Newtonian blood rheology (cf. Thurston [13]) as noted with distinguishable marks. All the curves are found to be decreasing from their maxima at the axis as one moves away from it and finally drop to zero on the wall

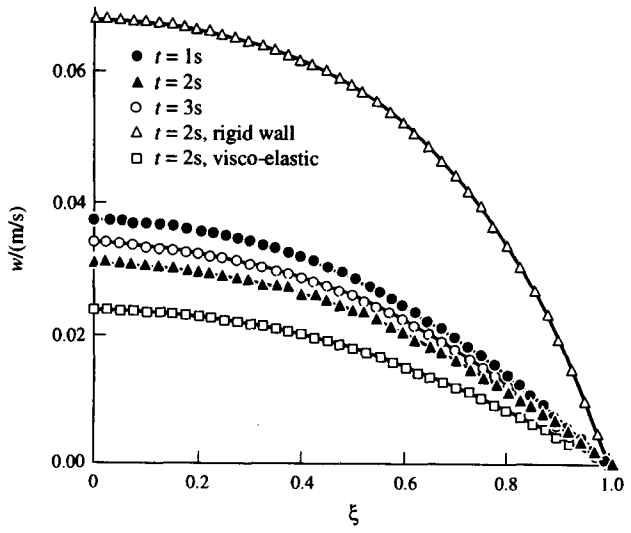

Fig. 2. Axial velocity profile for the parent artery at $z = 12.5$ mm for different time periods ($\tau_m = 0.4a$, $\beta = 30°$).

surface. The time-variant nature of the flow velocity reflects closely the input pulsatile pressure gradient, as anticipated. The flow velocity appears to enhance significantly in the absence of any vessel wall motion so that one can estimate the effect of the consideration of the wall motion on the flow velocity quantitatively through a direct comparison of the relevant curves of the figure. It is also observed that blood rheology affects the flow velocity mildly by reducing its magnitude to some extent. Thus one may conclude after a thorough study over the results of the present figure that both the vessel wall distensibility and non-Newtonian rheology of blood play important roles in such a bifurcated flow model.

Unlike the nature of the velocity profile in the parent aorta, the velocity profile of the flowing blood in the daughter arteries is changed drastically as observed from the results of Fig. 3 which consist of five different curves. Three similar curves with slight fluctuations corresponding to different time periods show their maxima near the inner wall followed by a back flow region in the vicinity of the inner wall and finally approach zero on the outer wall surface by traversing the path of positive non-zero values distal to the separation zone. The curve representing the

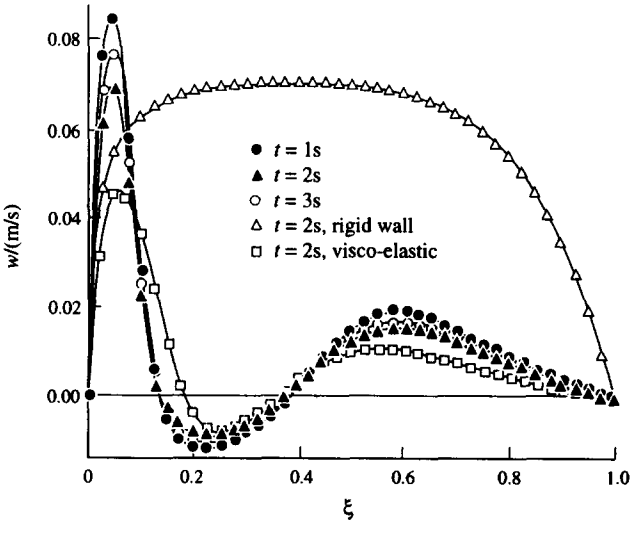

Fig. 3. Axial velocity profile for the daughter artery at $z = 40$ mm for different time periods ($\beta = 30°$).

results without the presence of the wall motion behaves in an entirely different way where no flow reversal occurs and it increases sharply from zero on the inner wall, attains a peak near the median wall surface and then gradually drops to zero on the outer wall. In contrast to this, the flow velocity is again found to attain a relatively low peak value near the inner wall surface and then declines gradually to zero on the outer wall with a back flow region when blood rheology is taken into account as noted from the nature of another curve of the current figure. Studying the results of Figs 1 and 2, it may be of some importance to note that the rheology of the flowing blood and the wall distensibility influence the velocity pattern in daughter arteries more than that in the parent aorta. Moreover, the present observation reveals that the rheology of blood or a non-Newtonian fluid representing blood is more resistant to flow changes from a forward flow to a reverse flow or vice versa. These results agree qualitatively well with the observations of Nakamura and Sawada [14, 15] who studied both the steady and the unsteady characteristics of stenosis with biviscosity fluid flow and remarked that the non-Newtonian property of blood diminishes, the distortion of the flow pattern tends to restrain the occurance and growth of flow separations in an accelerating flow and promotes the disappearance of flow separation in decelerating flow.

From the physiological point of view, since the bifurcation angle at the human aortic bifurcation changes between 10 and 80°, here the results for the axial velocity pattern at the apex for various bifurcation angles in the physiologic range at a particular instant of $t = 2$ s are shown in Fig. 4. The present figure also includes the results by incorporating blood rheology and by ignoring the wall distensibility under consideration, in order to have proper understanding of their influences on the velocity profile at the apex. It is observed that with the increase in the bifurcation angle, the usual velocity pattern of parabolic nature is perturbed considerably and gradually gets flattened. The bifurcation angle influences the Coriolis force considerably and the secondary flow is prominent in the present study because of a large bifurcation angle and a relatively flat flow profile. When the wall motion is totally withdrawn from the system under consideration the profile appears to have gained much higher magnitude with an entirely flattened top different from all other cases. Again the non-Newtonian rheology of blood does not drastically change the fluid dynamics at the aortic bifurcation as noted from the relevant curve of the present figure. Such observation agrees qualitatively well with those of Duncan *et al.* [16] and Lou and Yang [4, 17] where the former performed an experiment to understand the local effect of the wall distinsibility in arterial bifurcation while the later studied the same theoretically by computer simulation.

Figure 5 includes the velocity profile in the daughter arteries for different axial positions at a particular instant of $t = 2$ s. One observes from the results of the present figure that the velocity profile remains parabolic near the apex corresponding to $z = 35$ mm and as one moves away from the flow divider, the profile gets perturbed largely towards the inner wall surface while a stationary zone is formed at the outer wall vicinity. It is also observed that a complete reverse flow occurs towards the inner wall at $z = 45$ mm, that is a short distance to the right of the apex while distal to the apex viz. at $z = 55$ and 52.5 mm the reappearance of back flow takes place both in the vicinity of the inner wall and midway between the inner and outer wall of the branch artery. All such behaviours are caused by the secondary flow which is a spiral flow pattern from the outer to the inner wall in the bifurcation plane. From the physiological point of view, the secondary flow depends on the interplay among the viscous force, Coriolis force, other internal force and the axial pressure gradient. The Coriolis force is more uniformly distributed across the daughter arteries.

The results of the wall shear stress distributed over the parent aorta in the presence of stenosis for different time periods together with the influence of blood rheology and the wall distensibility on them are presented in Fig. 6. One may note that for all times the wall shear stress appears to gain its maximum magnitude at the critical site where the parent aorta assumes its maximum constriction and its pulsatile behaviour is responsible for the input

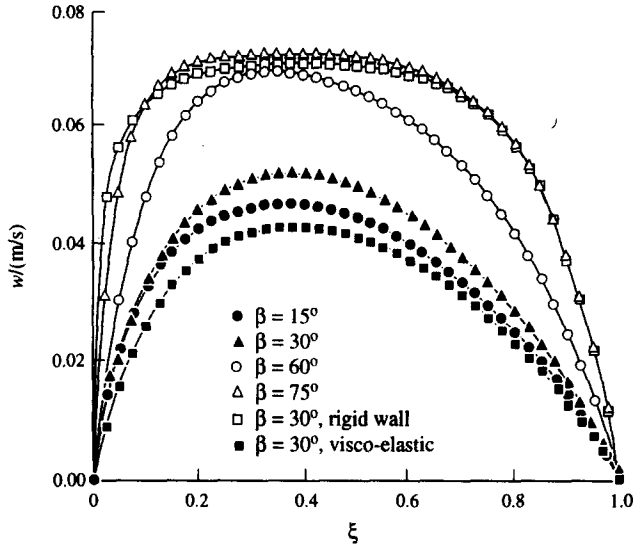

Fig. 4. Axial velocity profile at the apex for different values of β at $t = 2$ s.

pressure gradient of pulsatile nature. Moreover, for all the times considered in the present results the stresses are relatively higher proximal to maximal stenosis and lower distal to the stenosis due to flow separation. The symmetrical portion of the stress curve corresponding to the presence of stenosis becomes a straight line with constant stress in the absence of the constriction. When the rheology of blood is changed from Newtonian to non-Newtonian, the stress is enhanced considerably throughout the arterial segment under study. Again if the wall motion is totally disregarded, the stress curve is found to be symmetrical in the constricted area about the critical location of maximum constriction with an all time higher proximal to maximal stenosis and lower distal to the stenosis due to flow separation. However, their magnitudes are lowered to some extent throughout the artery. After examining all the results of the present figure one can conclude that maximum stresses occur at a point of minimal arterial cross section for all the cases and the deviations of maximum and minimum stresses are less for wall distensibility and more for blood rheology.

Figures 7 and 8 display the distributions of the shear stress over the outer and inner walls of

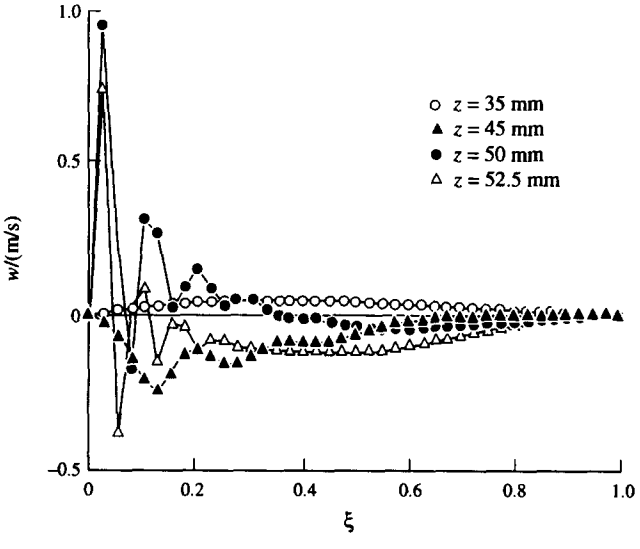

Fig. 5. Axial velocity profile for the daughter artery at different axial positions ($\beta = 30°$, $t = 2$ s).

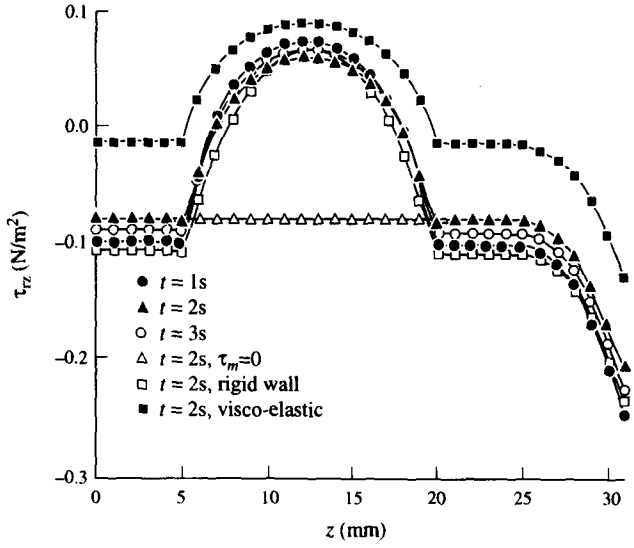

Fig. 6. Wall shear stress distribution for the parent aorta at different time periods ($\beta = 30°$).

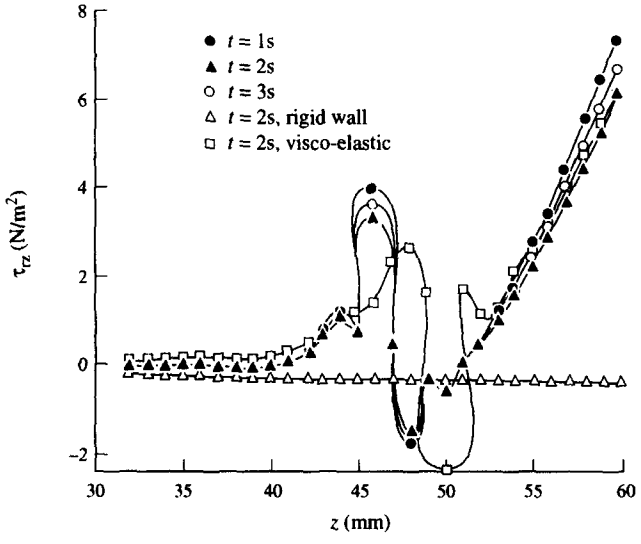

Fig. 7. Wall shear stress distribution for the daughter outer wall at different time periods ($\beta = 30°$).

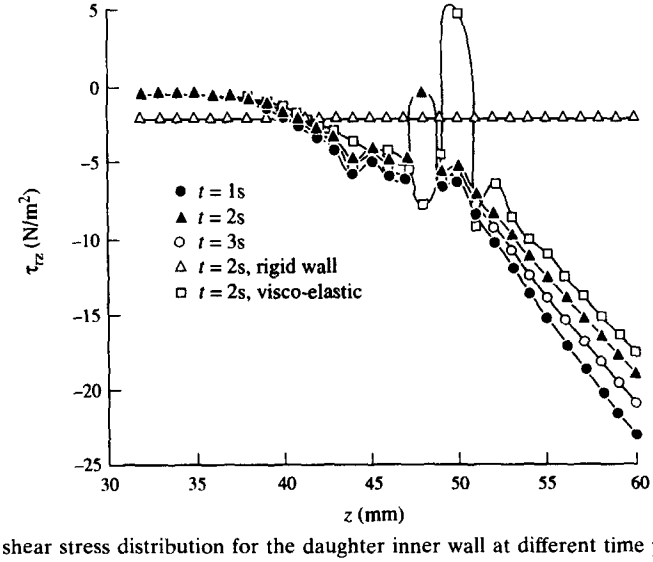

Fig. 8. Wall shear stress distribution for the daughter inner wall at different time periods ($\beta = 30°$).

the daughter artery for different time periods. One may record here that there are two distorted shear stress regions—one on the outer wall peaking at a point immediately distal to the lateral junction and the other on the inner wall peaking at a point distal to the flow divider or the apex. This observation is in good agreement again with that of Lou and Yang [4]. There have been two major hypotheses that relate to a possible hemodynamic role in atherogenesis—one is the low shear stress pointed out by Caro *et al.* [18] and the other is the high shear stress reported by Fry [19]. According to Fry [19], the degradation of some sort in canine walls may occur owing to a continuous exposure to a shear stress of 38 N/m^2 within a period of 1 hour. It is also observed from the present figures that the outer wall shear stress increases gradually from the vertex and it forms several recirculation zones in the vicinity of $z = 50$ mm followed by a positive non-zero value while it maintains negative stress on the inner wall including a disturbance near $z = 50$ mm. When the wall motion is withdrawn from the present flow mechanism, the shear stresses on both the inner and outer walls are reduced mildly throughout the arterial length under consideration. On the other hand, if blood rheology is taken into account, the stress curve for the outer wall appears to have some distortion and that for the inner wall claims to have a recirculation zone near $z = 50$ mm. It is worth noting that the sign of the wall shear stress becomes positive when the flow is forward and negative when the stream is reversed. Here too, the effect of wall distensibility of the shear stress for the daughter arterial walls is meagre while the blood rheology does influence both the inner and outer wall stresses of the daughter artery considerably.

The variation of the flow rate with time at a particular location of $z = 12.5$ mm where the constriction of the parent aorta is maximum, is depicted in Fig. 9. It appears that there is no considerable deviation of the flow rates in the parent aorta if the rheology of blood is changed from Newtonian to non-Newtonian as observed from a pair of closed bottom curves. However, in the absence of stenosis, that is, in the case of normal aorta, the flow rate gets accelerated rapidly in the systolic phase and decelerated in the diastolic phase of the first cardiac cycle and then it gradually follows a slightly upward trend with little fluctuations for the rest of the time. The deviation of the results thus obtained clearly estimates the effect of stenosis on the flow rate in the parent aorta bifurcating into two daughter arteries under consideration. Besides this, the blood rheology potentially contributes to the flow rate in the daughter arteries unlike that in the parent aorta as shown in Fig. 10. The flow rate in the daughter arteries is found to be higher than that in the parent aorta in general and it is accelerated more for a non-Newtonain

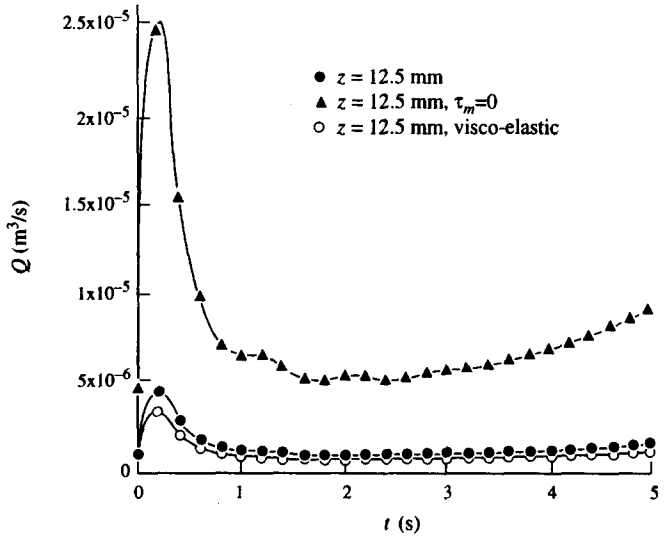

Fig. 9. Variation of the flow rate with time for the parent aorta at $\beta = 30°$.

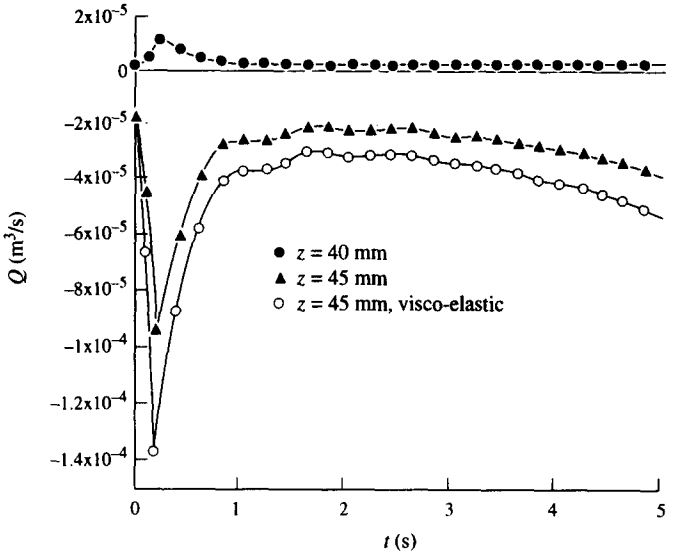

Fig. 10. Variation of the flow rate with time for the daughter artery at different axial positions ($\beta = 30°$).

fluid than for a Newtonian one representing blood, in particular. One may also notice that the flow rate becomes higher near the vertex than that at a location away from the flow divider. Moreover, it is worth noting that the flow rate becomes entirely positive due to the forward flow at $z = 40$ mm while its direction gets reversed at $z = 45$ mm as is evident in Fig. 10. All the curves of Figs 9 and 10 have a common feature in that they become steady to some extent immediately after expiry of the first cardiac cycle.

Figure 11 exhibits the variation of the wall shear stress with time in the parent aorta at $z = 12.5$ mm where the aorta assumes its maximum narrowing. Two more curves characterizing the shear stress, one in the absence of stenosis and the other with non-Newtonian fluid representing blood, are also included in this figure as noted with distinguishable marks. All such curves have their respective peaks towards the beginning followed by a sharp fall to become minimum at $t = 1$ s and then they remain almost invariant for the rest of the time excepting a marginal increasing trend towards the large passage of time as far as their magnitudes are concerned. It has been suggested that the change of shear stress direction or

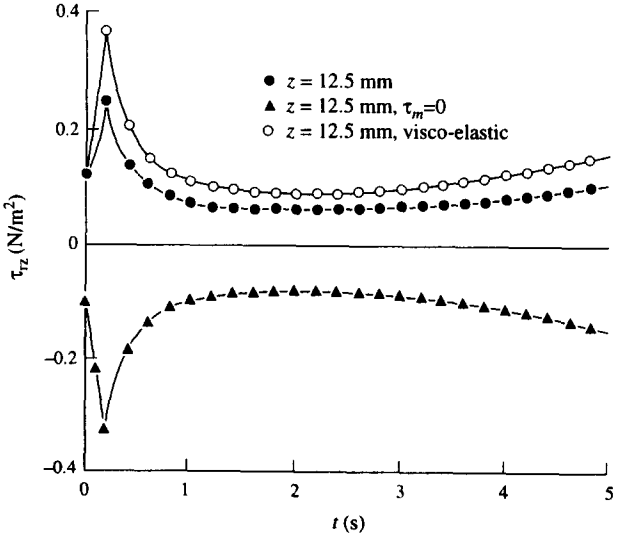

Fig. 11. Variation of the wall shear stress with time for the parent aorta at $\beta = 30°$.

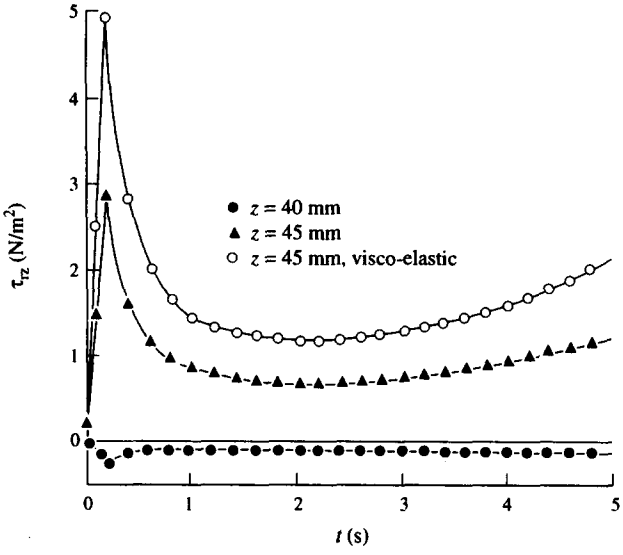

Fig. 12. Variation of the wall shear stress with time for the daughter outer wall at different axial positions ($\beta = 30°$).

amplitude within a cardiac cycle may be related to atherogenesis (cf. McDonald [20]). It has also been speculated by Fischer *et al.* [21] that the increased collagen production resulting from the pulsatile wall stretch due to the pulsatile pressure gradient may be an initiating event in vessel wall injury leading to atherogenesis. Thus, the observations made in the present figure agree with the hypothesis just stated and believed to provide some understanding regarding the formation of the arterial diseases leading to the malfunction of the circulatory system.

Finally, the concluding Figs 12 and 13 present the time variations of the shear stress on the outer and the inner walls of the daughter arteries respectively which also include the corresponding results for a non-Newtonian fluid representing blood. The stress characterizes to be positive on the outer wall and negative on the inner wall with much higher magnitude inducing flow separation on the inner wall of the branch artery for a Newtonian fluid at a location of $z = 45$ mm, but the nature of the stress remains invariant for both the outer and the inner wall at $z = 40$ mm. However, when non-Newtonian blood rheology is taken into

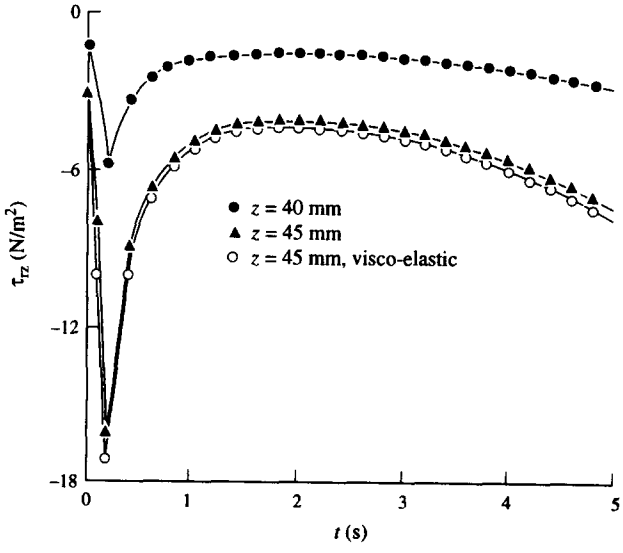

Fig. 13. Variation of the wall shear stress with time for the daughter inner wall at different axial positions ($\beta = 30°$).

consideration, the stress becomes positive on the outer wall and negative on the inner wall surface. Although the peak stress on the inner wall is found to be nearly 18% higher than that on the outer wall for a non-Newtonian fluid, even then the influence of blood rheology on the outer wall shear stress is more pronounced than that on the inner wall of the daughter arteries.

Acknowledgements—The authors are grateful to the Council of Scientific and Industrial Research for providing the financial assistance to carry out the present work. The authors are also grateful to the referees for their valuable comments and suggestions for the improvement of this paper.

REFERENCES

1. Liepsch, D. W. and Moravec, S. T., *Biorheology,* 1984, **21,** 571.
2. Liepsch, D. W., *Biorheology,* 1986, **23,** 395.
3. Lou, Z. and Yang, W. J., *Cric. Rev. Biomed. Engng,* 1992, **19,** 455.
4. Lou, Z. and Yang, W. J., *J. Biomech. Engng Trans. ASME,* 1993, **115,** 306.
5. Brown, N., Impedance matching at arterial bifurcations. *J. Biomech.,* 1993, **26,** 59.
6. Lessner, A., Zahavi, J., Silberberg, A., Frei, E. H. and Dreyfus, F., *Theoretical and Clinical Hemorheology* (ed. H. Hartert and A. L. Copley). Springer, New York, 1971, p. 194.
7. Thurston, G. B., *Biorheology,* 1973, **10,** 375.
8. Patil, M. K. and Subbaraj, K., *J. Biomech,* 1988, **21,** 219.
9. Nazemi, M., Kleinstreuer, C., Archie, J. P. and Sorrell, F. Y., *J. Biomech. Engng Trans. ASME,* 1989, **111,** 316.
10. Clark, M. E., Robertson, J. M. and Cheng, L. C., *J. Biomech.,* 1983, **16,** 895.
11. Burton, A. C., *Physiology and Biophysics of the Circulation.* Year Book Medical Publisher, Chicago, 1966.
12. Milnor, W. R., *Hemodynamics.* Williams & Williams, Baltimore, 1982.
13. Thurston, G. B., *J. Biomech.,* 1976, **9,** 13.
14. Nakamura, M. and Sawada, T., *J. Biomech. Engng Trans. ASME,* 1988, **110,** 137.
15. Nakamura, M. and Sawada, T., *J. Biomech. Engng. Trans. ASME,* 1990, **112,** 100.
16. Duncan, D. D., Bargeron, C. B., Borchardt, S. E., Deters, O. J., Gearhart, S. A., Mark, F. F. and Friedman, M. H., *J. Biomech. Engng Trans. ASME,* 1990, **112,** 183.
17. Lou, Z. and Yang, W. J., *Bio-Med. Mater Engng,* 1991, **1,** 173.
18. Caro, C. G., Fitz-Gerald, J. M. and Schroter, R. C., *Proc. R. Soc. Lond.,* 1971, **B177,** 109.
19. Fry, D. L., *Circ. Res.,* 1968, **22,** 165.
20. McDonald, D. A., *Blood Flow in Arteries.* 2nd ed. Edward Arnold, London, 1974.
21. Fischer, G. M., Swain, M. L. and Cherian, K., *Blood Vessels,* 1980, **17,** 215.

(Received 20 November 1995; in final form 13 June 1996)